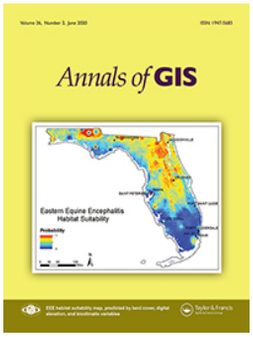

Taylor & Francis
Taylor & Francis Group

Annals of GIS

ISSN: (Print) (Online) Journal homepage: https://www.tandfonline.com/loi/tagi20

Freshwater lake inundation monitoring using Sentinel-1 SAR imagery in Eastern Uganda

Bernard Barasa & Joshua Wanyama

To cite this article: Bernard Barasa & Joshua Wanyama (2020) Freshwater lake inundation monitoring using Sentinel-1 SAR imagery in Eastern Uganda, Annals of GIS, 26:2, 191-200, DOI: 10.1080/19475683.2020.1743754

To link to this article: https://doi.org/10.1080/19475683.2020.1743754

Published online: 18 Mar 2020.

ANNALS OF GIS
2020, VOL. 26, NO. 2, 191–200
https://doi.org/10.1080/19475683.2020.1743754

Taylor & Francis
Taylor & Francis Group

Freshwater lake inundation monitoring using Sentinel-1 SAR imagery in Eastern Uganda

Bernard Barasa[a] and Joshua Wanyama[b]

[a]Department of Geography and Social Studies, Kyambogo University, Kyambogo, Kampala, Uganda; [b]Department of Agricultural and Bio Systems Engineering, Makerere University, Kampala, Uganda

ABSTRACT

In flood hazard assessment, little attention has been given to the seasonal observation of freshwater inundation using Sentinel-1 Synthetic-Aperture Radar (SAR) images in the tropics. To assess these spatial variations, this study examined the inundation magnitudes and reflectance of riparian flora in the raining seasons (February-April and September-November) and dry-periods (May-August and December-January). The inundation areas were determined using an object-oriented classification algorithm, whilst the merits concerning the lake, riparian vegetation and shoreline were well-defined using backscatter-coefficient values. Findings indicated that the SAR images are practical to monitor inundation coverages and discern lake basin specific features such as highland areas, shoreline, water and riparian-vegetation. Seasonally, inundated sizes were comparatively higher in February (902 sq. km) and October (700 sq.km). Backscatter values of inundated parts varied from −16 dB to −19 dB, whereas those of riparian vegetation were higher in the months of May and August. This study hence displays a clear-cut correlation between riparian-vegetation, hydrology and climate variables.

ARTICLE HISTORY
Received 19 July 2019
Accepted 11 March 2020

KEYWORDS
Lake inundation; Sentinel-1; SAR images; shoreline; backscatter-coefficient

1. Introduction

Spatial-temporal variations of lake inundation can cause hydrological, ecological and economic consequences (Yang et al. 2018). These can be as an outcome of high-water stages and wave action (Death, Fuller, and Macklin 2015; Sheng et al. 2016). Lake inundation can also trigger changes in chemical and morphometric characteristics such as the death of aquatic life and degradation of shoreline (Brito et al. 2017). To the adjacent neighbourhoods, inundated areas might also instigate loss of property and lives (Nsubuga et al. 2017; Tumusiime and Ageet 2018).

Disaster management activities in the developing countries are highly skewed concerning emergency response than preparedness and mitigation (Zhang and Werner 2015). As a result, the areas vulnerable to flooding witness loss of aquatic lives, people and livestock, destruction of building and farmlands, and relocation of victims. Therefore, there is a need for studies to explore the capabilities of using remote sensing data such as Sentinel-I SAR images in monitoring inundation during the wet and dry seasons. The challenges hindering disaster risk preparedness are attributable to inadequate information of lake behaviours such as variations of inundation extents and the hysteretic relationship with riparian vegetation. This is caused by limited application of SAR images in monitoring flood magnitudes attributable to lack of methodological proficiencies to extract disaster evidence and dissemination of early warning messages.

The use of SAR images has proven to be helpful in assessing the temporal variations of lake behaviours and vulnerabilities (Bates et al. 2005; Mason et al. 2010). This SAR technology has a high capability to routinely capture and store images through clouds and hazy atmospheric conditions like fog, smog, light rain, mist (Chapman et al. 2015). The SAR satellites also have the capacity to continuously monitor inundation occurrences because they can produce correct, quick and cost-effective lake inundation sizes that can inform disaster risk managers on damages and losses of property (Sass et al. 2012; Rahman and Thakur 2018).

However, most studies have applied SAR images in detecting surface water quality (Irwin et al. 2017) and investigating lake water fluctuations in intra-months (Zeng et al. 2017). Little consideration has been rendered to the monitoring of lake inundation extents in the wet and dry seasons in the tropics especially for the of small lakes that are illustrated by multifaceted morphologies and positioned in broad and wide network of permanent and seasonal wetland systems. Additionally, no published study has generated a pixel-based upland-shoreline-lake inundation longitudinal profile using SAR images.

CONTACT Bernard Barasa barasagis@gmail.com Department of Geography and Social Studies, Kyambogo University, Kyambogo, Kampala, Uganda

Examining the extent of inundation and lake morphology is significant in flood risk reduction and implementation of recovery programmes (Zhang and Werner 2015). The overarching objective of this research was to monitor the lake inundation extents during the wet and dry seasons in 2015 using Sentinel-1 SAR images. The specific objectives of this study were to (i) to develop a pixel-based upland-shoreline-lake inundation longitudinal profile and (ii) map the lake inundation magnitudes using SAR images.

2. Materials and methods

2.1 Description of the study area

The study area is located in the eastern part of Uganda, East Africa. At water management zonal level, the studied site is found in the Lake Kyoga Water Management Zone. Within Lake Kyoga basin, the freshwater lakes that were studied were Lake Bisina and Opeta. The lakes are placed on the eastern part of Lake Kyoga at an elevation of 1,032 metres above sea level (Figure 1). Lake Bisina is found at 01°38′29″ N and 033°56′04″ E, while Opeta at 01°38′39″ N 034°09′25″ E is found in the north-eastern part of Uganda and shadow of Mt. Elgon.

Lake Bisina is a shallow lake that develops and shrinks depending on rainfall, but in a typical year covers about 150 km^2 with a mean depth of 3 metres and a maximum of 5 metres (Gidudu et al. 2011). The key tributaries contributing significant water inflows to Lake Bisina are Rivers Lokok and Lokere, while to Lake Opeta is Kelim River. Lokok and Lokere Rivers originate from the highlands found in Karamoja region whereas Kelim originates from the Mpologoma wetland system.

Topographically, the lakes are situated in an area of local depression such that any runoff from upstream areas contributes to lake storage and inundation. The study area experiences a bimodal rainfall pattern (Conway et al. 2005). The lakes receive rainfall totals that range from 850–1500 mm per annum received in two seasons; February-April and September-November and dry season between May-August and December-

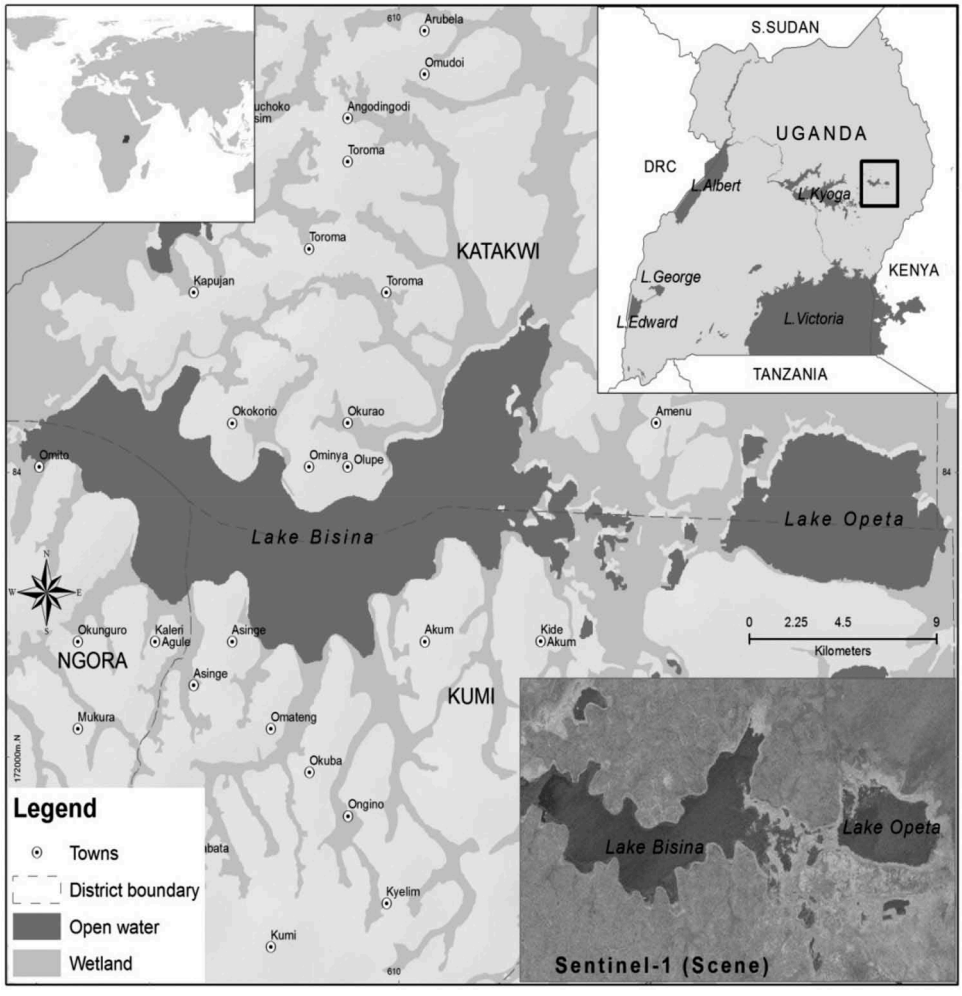

Figure 1. Location of lake Bisina and Opeta.

January. The lakes record a mean annual maximum temperature of 31.6°C experienced in January and a mean minimum of 17°C in October.

The soils of the areas adjacent to both lakes are comprised of ferrasols, nitosols and acrisols Lithologically. Geologically, the lakes lie on the basement complex of a pre-cambrian rock that includes granites, mignalites, gneiss, schists and quartzites. The upland vegetation is mainly made of savannah characterized by woodlands, grass, bushes and riparian.

The shallow freshwater lakes are surrounded by a vast and thin strip of fringing papyrus swamps (Wanda et al. 2011) and an extensive swamp of Vossia cuspidate to the east and south graduating into dry *hyparrhenia* grassland savannas (Amaniga Ruhanga and Iyango 2010). The lakes are connected with a fringing papyrus stretch which is approximately 9.7 km. The majority of riparian vegetation species in both lakes is submerged, and the rest floating-leafed plants. Nymphaea caerulea is far the most prevalent floating-leaf plant while *Najas horrida* was the most prevalent submersed plant followed by *Ceratophyllum demersum* and *Potamogeton schweinfurthii* (Gidudu et al. 2011). Water depths, altitude, and rainfall are the most critical environmental variables that influence vegetation distribution and species assemblages in the Lakes Opeta and Bisina (Ssegawa et al. 2004).

2.2 Cross-sectional profile of Lake Opeta and Bisina

The Shuttle Radar Topography Mission (SRTM) Digital Elevation Model of 30 m spatial resolution was acquired, pre-processed and used to create the profile (stack profile tool) in ArcGIS software version 10.3. Figure 2 shows that lakes share the same bottom elevation ranges. The lakes are separated by undulating depressions with peak elevations that are filled with water and riparian floating vegetation on the surface. The generated profile spans 45,000 m across the studied lakes.

2.3 Data acquisition of Sentinel-1 SAR images

SENTINEL-1 SAR multi-temporal images (C-band) were acquired from the Sentinel Scientific Data Hub (https://scihub.esa.int/dhus/) distributed by the European Space Agency. The images were defined by an Interferometric Wide Swath (IW) Mode features 5 x 20-metre spatial resolution and a 250 km (160 mi) swath.

This study interpreted the available and complete scene images of 2015 captured during the wet and dry seasons experienced by the area of study (Table 1). The SAR images were preferred for detecting the extent of lake inundation and its associated riparian vegetation because the images are available and freely accessible for downloading and interpretation. The 12-day revisit time is moderate to monitor inundation extents and associated lake dynamics.

Sentinel series represent the devoted space segment of the Global Monitoring Environment and Security (GMES) European programme. SENTINEL-1 is a C-band imaging Synthetic Aperture Radar (SAR) mission comprising a pair of satellites aimed at providing an all-weather (day and night) supply of imagery for GMES user services (Regan et al. 2010).

The SENTINEL-1 constellation provides high reliability, improved revisit time, geographical coverage and rapid data dissemination to support operational applications in the priority areas of marine and land monitoring, and emergency services (Torres et al. 2012). More details on satellite description, instrument payload, data products and application are described by Potin et al. (2012) and SENTINEL-1 User Handbook (2013).

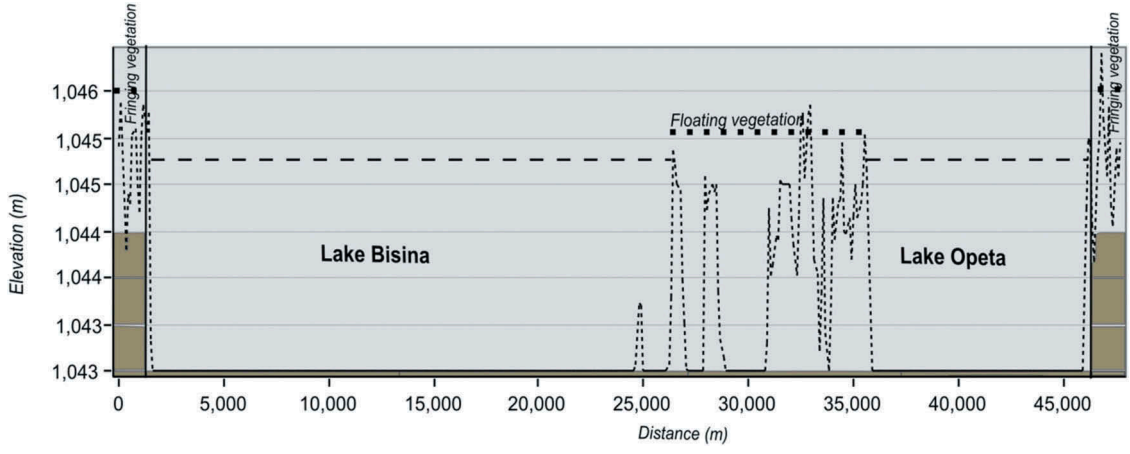

Figure 2. River channel cross-sectional profile from lake Bisina to Opeta (Shuttle Radar Topography Mission (SRTM) digital elevation model of 30 m).

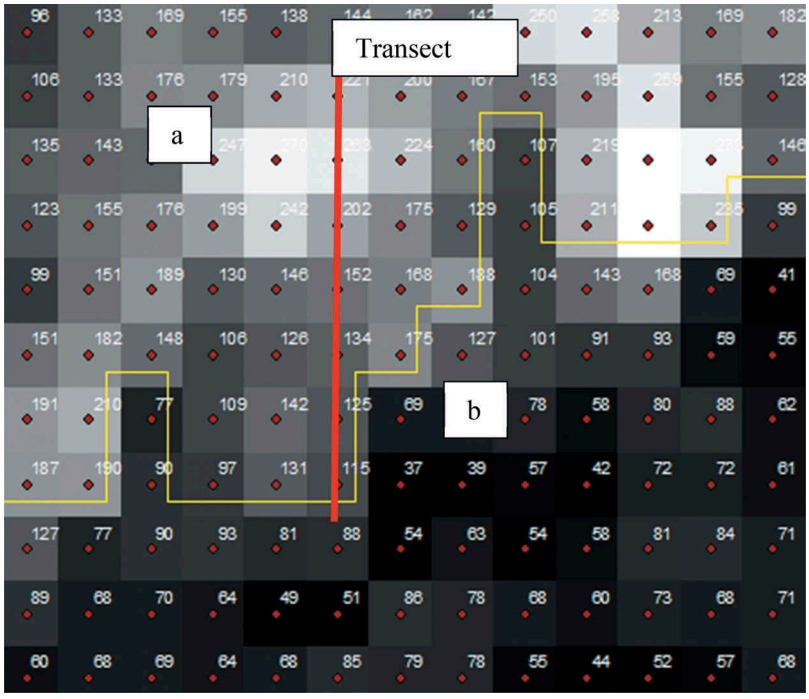

Figure 3. Pixel and segment assessment (a) shoreline and (b) open water.

2.4 Data processing

The SENTINEL-1 SAR images were pre-processed using the SENTINEL-1 toolbox (S1TBX). The toolbox consists of a collection of processing tools, data product readers and writers and a display and analysis application to support the large achieve of data from European Space Agency – SAR missions including SENTINEL-1, ERS-1 and 2 and ENVISAT, as well as third-party SAR data from ALOS PALSAR, TerraSAR-X, COSMO-SkyMed and RADARSAT-2 (Snoeij et al. 2009) . The downloaded image scenes were geometrically corrected using the terrain data with Range-Doppler terrain correction. The correction was based on an SRTM 3 Sec digital elevation model which was automatically downloaded and resampled using bilinear interpolation whereas the images were resampled using the nearest neighbourhood. These were geocoded to WGS 84/UTM zone 36 N at 10 m pixel spacing. The digital elevation model was used to remove the terrain-induced geometric distortions.

Subsets of corrected images were created from defined subsets covering approximate areas that are inundated by both Lake Bisina and Opeta. The subsets were created to improve rendering, pre-processing and processing efficiency. The SAR images were radiometrically calibrated to improve the Sigma output bands because the quality of the images is affected by terrain undulations (Loew and Mauser 2007). This was also vital for the derivation of mean backscatter coefficients (0) from the inundated, shoreline and fringing vegetation.

The scenes were filtered using a single product speckle filter (mean 3 × 3) method. The filter has a kernel size of 3 × 3 pixels and yields a speckle reduced image. This was applied to reduce the high-frequency noise that results from many randomly distributed point scatterers in a resolution cell (Martinis et al. 2015).

2.5 Lake inundation mapping

The extent of the water body and emergent riparian vegetation can be assessed by the SAR C-band (Bartsch et al. 2012). The pre-processed SAR images were classified using an image segmentation algorithm (mean shift) in Envi software 4.5. This procedure controls the shape and size of polygons upon tile portioning of images. Defined lake segments were selected and extracted for collation and validation (Figure 3). The segmented flood and shoreline areas were validated in the field following a visual inspection to assess their locational accuracy (Zhang et al. 2008). The extracted segments were matched with field locational data to assess how well the observed lake extents were representative.

2.6 Backscatter coefficient assessment

Backscatter coefficient assessment was performed to determine the distinction between the lake, riparian vegetation and shoreline using image digital numbers that were converted into backscatter coefficients (s°) for

Table 1. Specifications of acquired SENTINEL-1 SAR images for the year 2015.

Satellite	Specifications	Season	Year	Acquisition dates
Sentinel-1	Instrument: **SAR-C**			
	Mode: **IW**			
	Acquisition Type: **NOMINAL**	Dry		2015-06-4
	Cycle number: **61**		2015	2015-08-15; 2015-08-29
	Format: **SAFE**			
	Pass direction: **DESCENDING**			2015-05-1; 2015-05-11; 2015-04-07;
	Polarization: **VV**	Wet	2015	2015-03-24; 2015-03-14; 2015-09-08
	Product class: **S**			2015-10-02; 2015-10-16; 2015-10-26
	Product class description: **SAR**			
	Product composition: **Slice**			
	Product level: **L1**			
	Product type: **SLC**	Mission type: **Earth observation**		
	Slice number: **3**	NSSDC identifier: **0000-000A**		
	Start relative orbit number: **50**	Operator: **European Space Agency**		
	Status: **ARCHIVED**			
	Stop relative orbit number: **50**			
	Azimuth spacing: **9.9 m**			
	Radar frequency: **5.4 MHz**			

absolute comparisons of polarizations of the backscattering behaviour (Williams et al. 2014). This is represented by the standard equation:

$$\sigma^{\circ} = 10\log_{10}[a_2(DN^{20-}{}_{a1}N_{(r)})] = dB$$

The backscatter value ranges were used to interpret the lake seasonal inundation, riparian vegetation and shoreline variations. The same parameters were assessed during both the rainy and dry seasons to accurately determine their locations, reflectance, extents and qualify the capabilities of SAR images.

2.7 Image performance assessment

The SAR image abilities were examined using mapped inundation extents in relation to field observations with the help of handheld Global Positioning Systems in areas of reach. A total of 302 positional locations were mapped from the referenced lakeshore to the endpoint of the flood extent. In addition, to confirm the potential of images in representing water bodies and shoreline, a Shuttle Radar Topogra phy Mission (SRTM) data was acquired and used. The overall image classification accuracy obtained in the dry season was 83% while in the wet season was 88% (Table 2).

The SRTM Water Body Data published on 1 February 2002 was acquired (http://earthexplorer.usgs.gov/) and superimposed with the segmented lake and inundation extents. This data facilitated the identification of water bodies and the delineation of shorelines in each 1 × 1 cell. Furthermore, a land cover water layer was also obtained from the Ministry of Water and Environment for the year 2010 to support the identification of water bodies in image mosaics through overlays in the classification process (Slater et al. 2006; Bartsch et al. 2009).

3. Results

3.1 Pixed-based upland-shoreline-lake inundation longitudinal profiling

This result revealed that the lakes were seasonally inundated in space and time. From the image pixels examined, upland areas had relatively higher pixel values than the lake shoreline and water body (Figure 4). The upland areas and shoreline had a relatively higher peak of the longitudinal profile than the inundated area. This finding further shows that within the inundated area, the profile variations were attributable to the interactions between riparian vegetation and water.

Table 2. Image classification accuracy assessment in dry and wet season seasons.

Parameters	Lake	Riparian Vegetation	Shoreline	Upland areas
Dry season				
Lake	68	2	0	6
Riparian Vegetation	5	62	1	4
Shoreline	5	3	61	3
Upland areas	7	6	6	63
User accuracy	80	84.93	89.71	82.89
Overall accuracy %	*83.1*			
Kapa statistics	*0.79*			
Wet season				
Lake	77	5	3	1
Riparian Vegetation	5	68	1	8
Shoreline	0	3	60	3
Upland areas	4	4	3	57
User accuracy	89.53	85	89.55	82.61
Overall accuracy %	*88.8*			
Kapa statistics	*0.82*			

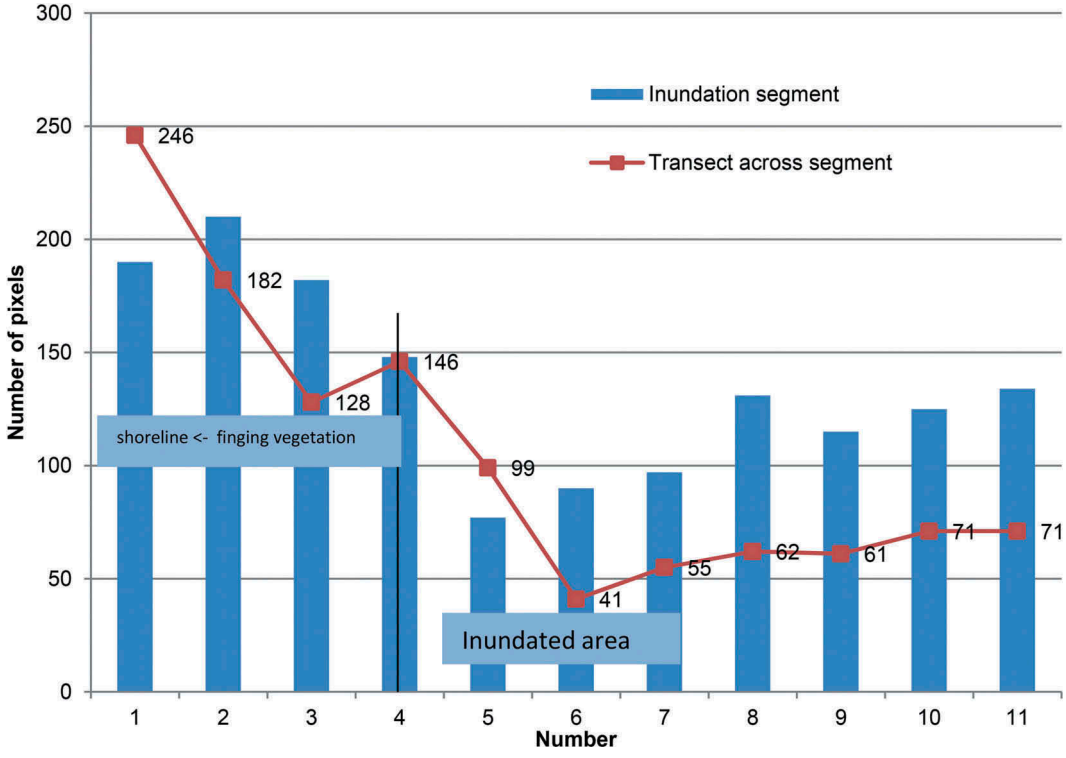

Figure 4. Pixel and segment-based inundation and shoreline monitoring.

3.2 Lake inundation and riparian vegetation assessment

Within the backscatter value ranges, the lake had lower values during the first rainy season (February-April) than in the second wet season (September–November). The flooded areas posted backscatter values ranging from −16 and −19 dB, while in the dry season the values were between −15 and −1 dB (Figure 5).

This study further reveals a high receding of floodwaters in the month of May from the last intensive rains until September when the lake inundates again. The December-January dry season seemed not to have a significant impact on the reduction of inundation extents as compared to the second dry season (May–August). The same backscatter values were used to interpret the variations in riparian fringing vegetation.

The reflectance of riparian vegetation was moderately higher in the dry season especially in the months of May and August compared to the rainy months. The dry season played a significant role in the increment and distribution of riparian vegetation magnitudes. However, it is only the second wet season (September–November) which experiences a rise in the size of riparian vegetation. As per the plotted backscatter values, the difference

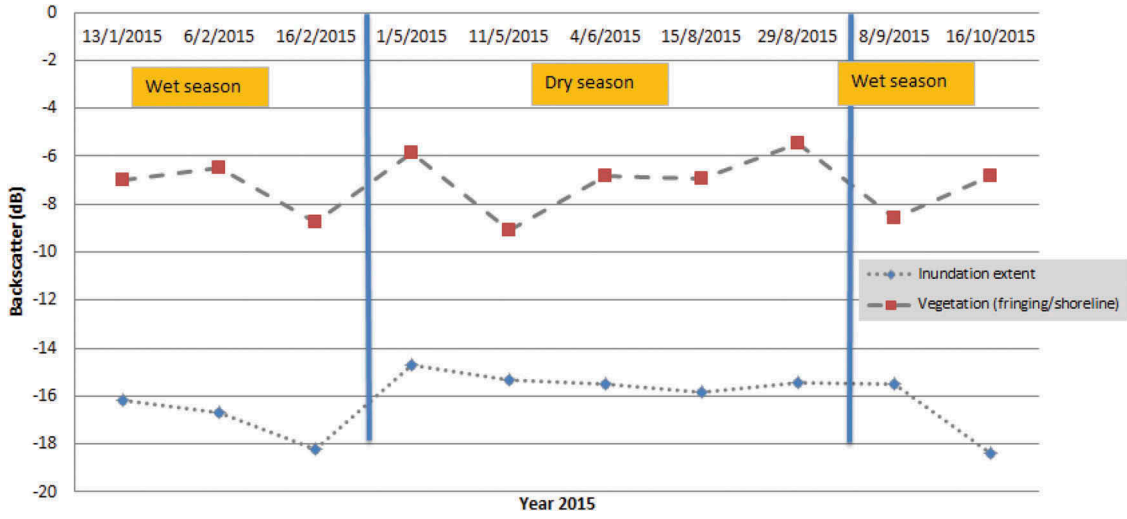

Figure 5. Backscatter of seasonal variations of lake inundation and riparian vegetation.

between inundated areas and riparian fringing vegetation was −5 dB.

3.3 Mapping of lake inundation extent

In the studied period, the highest extents of lake inundation were basically experienced in both rainy seasons i.e. February-April and September-November (Figure 6). Figure 7 shows the seasonal extents of lake inundation for the months of August (bottom) and October (top) 2015. Within these assessments, the highest inundation size mapped was experienced in the first rainy season (February-April) with the peak in the month of February (902 sq.km); while in the second wet season (September-November), the largest flood extent recorded was 700 sq.km experienced in the month of October. The magnitude of fringing vegetation was higher in the first dry season (May-August) than in the second dry season (December-January).

4. Discussion

This study on a local area is described with small freshwater lakes and frequent floods. Understanding recurrent lake inundation disparities is of global importance for practitioners to take advantage of exploiting satellite images in the zoning of disasters and dissemination of early warning information.

The first result of this study is hinged on the capacity to use SAR image pixel values to develop transects that can be used in examining synergies between upland areas and water bodies in inundation monitoring. The

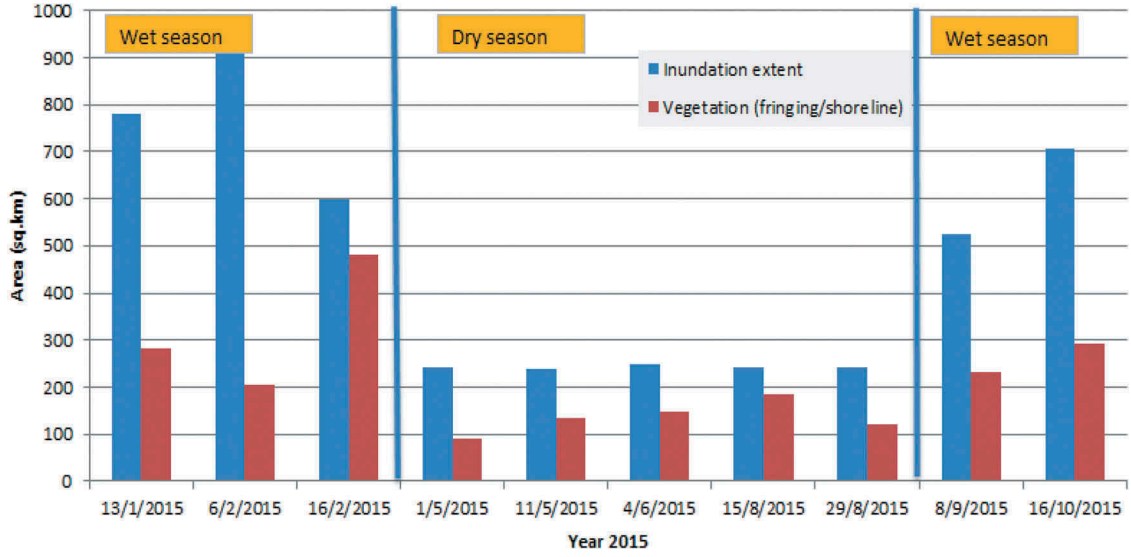

Figure 6. Seasonal lake inundation extents.

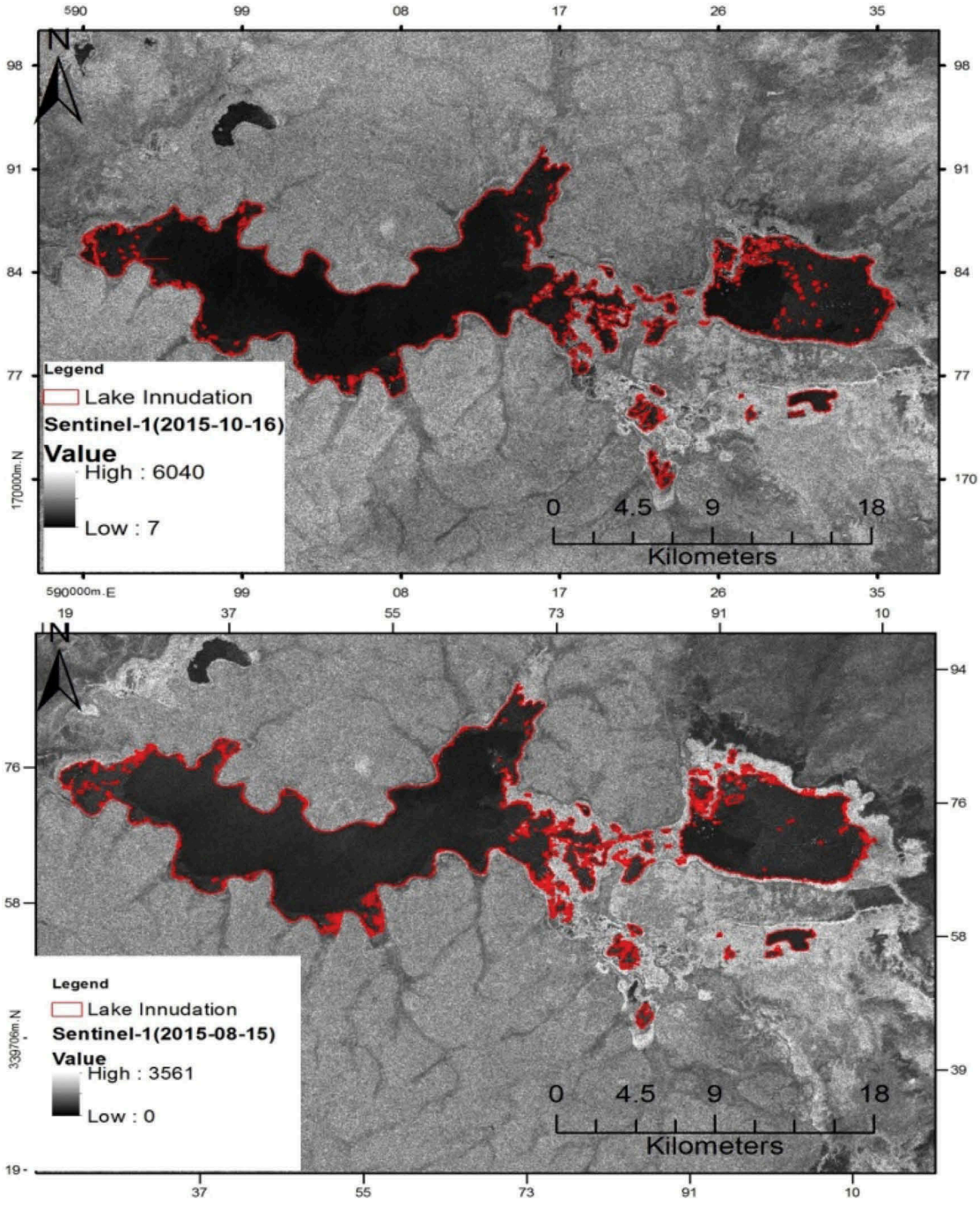

Figure 7. Seasonal lake inundation extents for the months of August (bottom) and October (top) 2015.

developed profile was defined by a decreasing trend from upland areas to places with fringing vegetation, though it finally declines in the water body. This finding could be caused by high absorption of water and reflectance of the emitted radiation by riparian fringing vegetation and upland areas. This might have been expected but the usability of pixel values in investigating profiles of lacustrine wetlands and lakes located in floodplain areas is re-affirmed.

The second key result of this study is that within the backscatter value ranges, Lake water values recorded were slightly lower during the first rainy season (February–April) than in the second season (September–October). The first rainy period experiences higher concentrations of riparian fringing vegetation and chlorophyll in the water that absorbs more radiation. The prolonged dry season (May-August) facilitates colonization of riparian vegetation due to high temperatures,

wave action and prevalence of strong winds on the lakes. The December-January dry season seems not to have a significant impact on the reduction of inundation extents as compared to the second dry season (May–August). This is so especially because the lakes are surrounded by a broad and wide network of permanent and seasonal wetland systems that have regulated flow into the lakes. In addition, the study shows that riparian vegetation is highly sensitive to hydrological regimes which are in consonance with Nones and Varrani (2016). The reflectance of riparian vegetation was moderately higher in the dry season especially in the months of May and August. This finding could be attributed to high colonization of water bodies by the invasion of exotic water weeds and high availability of nitrogen. However, it is worthy to note that the riparian vegetation could increase subsurface water storage due to reduced evapotranspiration that also improved the productivity of the lake.

The third key result of this research is that within these assessments, the highest inundation size mapped was experienced in the first rainy season (February–April) with the peak seen in the month of February; while in the second rainy period, the largest flood extent recorded was experienced in the month of October. This finding was expected primarily because the study receives high and longer rains in the first rainy season.

However, the extents of inundation of studied freshwater lakes had not been quantified before. This study clearly demonstrates the capabilities of using SAR images in quantifying inundation areas, monitoring of riparian fringing vegetation and shoreline in freshwater lakes. This finding can guide policymakers in the allocation and distribution of resources meant for disaster risk reduction, recovery and water resources management at the lake basin scale.

5. Conclusion

This study demonstrates the abilities to use SAR image pixel values to develop transects that can be used in examining synergies between upland areas and water bodies in disaster monitoring. This research proves substantial evidence that SAR C-band images are appropriate in flood mapping exercises and monitoring riparian vegetation in inaccessible areas. The areas inundated had backscatter values ranging from −16 dB and −19 dB. The backscatter difference between inundated areas and riparian vegetation was −5 dB. This is due to the high presence of riparian vegetation on the lakes. This finding is also important in monitoring the presence of riparian vegetation, its growth and implications on water resources and survival of aquatic life. The highest inundation extent mapped was experienced in February and October. This study also reveals that there is a complex relationship between riparian vegetation, hydrology and climate variables. The utilized mapping procedure of segmentation is rigorous and can be used widely to monitor inundation extents; it shows high contrasts between water, vegetation and land surfaces.

Disclosure Statement

The authors have no hidden interests in the publication of this article

Funding

This work was supported by the ESA Tiger capacity building facility programme hosted at The International Institute for Geo-Information Science and Earth Observation, Netherlands.

References

Amaniga Ruhanga, I., and L. Iyango. 2010. "A Socio-economic Baseline Survey of Communities Adjacent to Lake Bisina/Opeta and Lake Mburo/Nakivali Wetland Systems." Providing Baseline Information for the Implementation of the COBWEB Project in Western and Eastern/North-Eastern Uganda, Nature Uganda, Kampala, Uganda, 65.

Bartsch, A., A. M. Trofaier, G. Hayman, D. Sabel, S. Schlaffer, D. B. Clark, and E. Blyth. 2012. "Detection Of Open Water Dynamics with Envisat Asar in Support Of Land Surface Modelling at High Latitudes." *Biogeosciences* 9 (2): 703-714. doi:10.5194/bg-9-703-2012.

Bartsch, A., W. Wagner, K. Scipal, C. Pathe, D. Sabel, and P. Wolski. 2009. "Global Monitoring of Wetlands–the Value of ENVISAT ASAR Global Mode." *Journal of Environmental Management* 90 (7): 2226–2233. doi:10.1016/j.jenvman.2007.06.023.

Bates, P. D., M. S. Horritt, D. Cobby, and D. Mason. 2005. "Flood Inundation Modelling Using LiDAR and SAR Data." *Spatial Modelling of the Terrestrial Environment*. doi:10.1002/0470094001.ch5.

Brito, B. C., B. R. Forsberg, D. Kasper, J. H. Amaral, M. R. de Vasconcelos, O. P. de Sousa, W. R. Bastos, and W. R. Bastos. 2017. "The Influence of Inundation and Lake Morphometry on the Dynamics of Mercury in the Water and Plankton in an Amazon Floodplain Lake." *Hydrobiologia* 790 (1): 35–48. doi:10.1007/s10750-016-3017-y.

Chapman, B., K. McDonald, M. Shimada, A. Rosenqvist, R. Schroeder, and L. Hess. 2015. "Mapping Regional Inundation with Spaceborne L-Band SAR." *Remote Sensing* 7 (5): 5440–5470. doi:10.3390/rs70505440.

Conway, D., E. Allison, R. Felstead, M. Goulden, T. Spencer, A. S. Laughton, and N. C. Flemming. 2005. "Rainfall Variability in East Africa: Implications for Natural Resources Management and Livelihoods." *Philosophical Transactions of the Royal Society A: Mathematical, Physical and Engineering Sciences* 363 (1826): 49–54. doi:10.1098/rsta.2004.1475.

Death, R. G., I. C. Fuller, and M. G. Macklin. 2015. "Resetting the River Template: The Potential for Climate-related Extreme Floods to Transform River Geomorphology and Ecology."

Freshwater Biology 60 (12): 2477–2496. doi:10.1111/fwb.2015.60.issue-12.

Gidudu, B., R. S. Copeland, F. Wanda, H. Ochaya, J. P. Cuda, and W. A. Overholt. 2011. "Distribution, Interspecific Associations and Abundance of Aquatic Plants in Lake Bisina, Uganda." *Journal of Aquatic Plant Management* 49: 19.

Irwin, K., D. Beaulne, A. Braun, and G. Fotopoulos. 2017. "Fusion of SAR, Optical Imagery and Airborne LiDAR for Surface Water Detection." *Remote Sensing* 9 (9): 890. doi:10.3390/rs9090890.

Loew, A., and W. Mauser. 2007. "Generation of Geometrically and Radiometrically Terrain Corrected SAR Image Products." *Remote Sensing of Environment* 106 (3): 337–349. doi:10.1016/j.rse.2006.09.002.

Martinis, S., and C. Rieke. 2015. "Backscatter Analysis Using Multi-Temporal and Multi-Frequency SAR Data in the Context of Flood Mapping at River Saale, Germany." *Remote Sensing* 7 (6): 7732–7752. doi:10.3390/rs70607732.

Mason, D. C., R. Speck, B. Devereux, G. J. P. Schumann, J. C. Neal, and P. D. Bates. 2010. "Flood Detection in Urban Areas Using TerraSAR-X." *IEEE Transactions on Geoscience and Remote Sensing* 48 (2): 882–894. doi:10.1109/TGRS.2009.2029236.

Nones, M., and A. Varrani. 2016. "Sensitivity Analysis of a Riparian Vegetation Growth Model." *Environments* 3 (30): 1–15. doi:10.3390/environments3040030.

Nsubuga, F. W., J. O. Botai, J. M. Olwoch, C. J. deW Rautenbach, A. M. Kalumba, P. Tsela, K. F. Mearns, A. A. Sentongo, and K. F. Mearns. 2017. "Detecting Changes in Surface Water Area of Lake Kyoga Sub-basin Using Remotely Sensed Imagery in a Changing Climate." *Theoretical and Applied Climatology* 127 (1–2): 327–337. doi:10.1007/s00704-015-1637-1.

Potin, P., P. Bargellini, H. Laur, B. Rosich, and S. Schmuck. July 2012. "SENTINEL-1 Mission Operations Concept." Geoscience and Remote Sensing Symposium (IGARSS), 2012 IEEE International, Munich, Germany, IEEE, 1745–1748.

Rahman, M. R., and P. K. Thakur. 2018. "Detecting, Mapping and Analysing of Flood Water Propagation Using Synthetic Aperture Radar (SAR) Satellite Data and GIS: A Case Study from the Kendrapara District of Orissa State of India." *Egyptian Journal of Remote Sensing and Space Science* 21: S37–S41. doi:10.1016/j.ejrs.2017.10.002.

Regan, A., P. Silvestrin, D. Fernandez, A. Gabriele, and N. Leveque. June, 2010. "Sentinel Convoy: Synergetic Observations with Satellites Flying in Formation with European Operational Missions." Small Satellite and Services Symposium (4S), Madeira, Portugal.

Sass, G. Z., M. Wheatley, D. A. Aldred, A. J. Gould, and I. F. Creed. 2012. "Defining Protected Area Boundaries Based on Vascular-plant Species Richness Using Hydrological Information Derived from Archived Satellite Imagery." *Biological Conservation* 147 (1): 143–152. doi:10.1016/j.biocon.2011.12.025.

Sheng, Y., C. Song, J. Wang, E. A. Lyons, B. R. Knox, J. S. Cox, and F. Gao. 2016. "Representative Lake Water Extent Mapping at Continental Scales Using Multi-temporal Landsat-8 Imagery." *Remote Sensing of Environment* 185: 129–141. doi:10.1016/j.rse.2015.12.041.

Slater, J. A., G. Garvey, C. Johnston, J. Haase, B. Heady, G. Kroenung, and J. Little. 2006. "The SRTM Data "Finishing" Process and Products." *Photogrammetric Engineering and Remote Sensing* 72 (3): 237–247. doi:10.14358/PERS.72.3.237.

Snoeij, P., E. Attema, A. Pietropaolo, V. Mastroddi, M. L'Abbate, and C. Bruno. 2009. Analysis of Sentinel-1 mission capabilities. In 2009 IEEE International Geoscience and Remote Sensing Symposium, vol. 1, pp. I-40. IEEE

Ssegawa, P., E. Kakudidi, M. Muasya, and J. Kalema. 2004. "Diversity and Distribution of Sedges on Multivariate Environmental Gradients." *African Journal of Ecology* 42 (s1): 21–33. doi:10.1111/aje.2004.42.issue-s1.

Torres, R., P. Snoeij, D. Geudtner, D. Bibby, M. Davidson, E. Attema, … I. N. Traver. 2012. "GMES Sentinel-1 Mission." *Remote Sensing of Environment* 120: 9–24. doi:10.1016/j.rse.2011.05.028.

Tumusiime, M. D., and S. Ageet. 2018. "Assessment of Impacts of Climate Change on Hydro-meteorological Ecosystem Services and Water Stress in Lake Kyoga Catchment." *International Journal of Research and Engineering* 5 (4): 345–354. doi:10.21276/ijre.

Wanda, F., B. Gidudu, S. Wandera, R. S. Copeland, J. P. Cuda, and W. A. Overholt. 2011. "Herbivory of Hydrilla Verticillata by Cichlid Fish in Lake Bisina, Uganda." *Journal of East African Natural History* 100 (1&2): 113–122. doi:10.2982/028.100.0107.

Williams, D., P. LeDantec, M. Chabot, A. Hillman, K. James, R. Caves, … Y. Wu. 2014. "RADARSAT-2 Image Quality and Calibration Update." EUSAR 2014; 10th European Conference on Synthetic Aperture Radar, Berlin, Germany, VDE, 1–4.

Yang, K., Z. Yu, Y. Luo, Y. Yang, L. Zhao, and X. Zhou. 2018. "Spatial and Temporal Variations in the Relationship between Lake Water Surface Temperatures and Water quality-A Case Study of Dianchi Lake." *Science of the Total Environment* 624: 859–871. doi:10.1016/j.scitotenv.2017.12.119.

Zeng, L., M. Schmitt, L. Li, and X. X. Zhu. 2017. "Analysing Changes of the Poyang Lake Water Area Using Sentinel-1 Synthetic Aperture Radar Imagery." *International Journal of Remote Sensing* 38 (23): 7041–7069. doi:10.1080/01431161.2017.1370151.

Zhang, Q., and A. D. Werner. 2015. "Hysteretic Relationships in Inundation Dynamics for a Large Lake–floodplain System." *Journal of Hydrology* 527: 160–171. doi:10.1016/j.jhydrol.2015.04.068.

Zhang, X., L. Jiao, F. Liu, L. Bo, and M. Gong. 2008. "Spectral Clustering Ensemble Applied to SAR Image Segmentation." *IEEE Transactions on Geoscience and Remote Sensing* 46 (7): 2126–2136. doi:10.1109/TGRS.2008.918647.